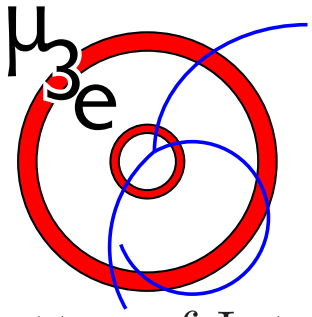

Letter of Intent for an Experiment to Search for the Decay $\mu \to eee$

A. Blondel, A. Bravar, M. Pohl
Département de physique nucléaire et corpusculaire, Université de Genève, Genève

S. Bachmann, N. Berger, A. Schöning, D. Wiedner
Physikalisches Institut, Universität Heidelberg, Heidelberg

P. Fischer, I. Perić
Zentralinstitut für Informatik, Universität Heidelberg, Mannheim

M. Hildebrandt, P.-R. Kettle, A. Papa, S. Ritt
Paul Scherrer Institut, Villigen

G. Dissertori, Ch. Grab, R. Wallny
Eidgenössiche Technische Hochschule Zürich, Zürich

P. Robmann, U. Straumann
Universität Zürich, Zürich

January 23^{rd}, 2012

Contents

Executive Summary

We propose an experiment (*Mu3e*) to search for the lepton flavour violating (LFV) decay $\mu^+ \to e^+e^-e^+$. We aim for a sensitivity of one in 10^{16} μ-decays, four orders of magnitude better than previous searches. This sensitivity is made possible by exploiting modern tracking detectors based on monolithic active pixel sensors providing high spatial resolution and hodoscopes using scintillating fibres and tiles providing precise timing information at high particle rates.

Existing beamlines available at PSI providing rates of order 10^8 muons per second would allow one to test the decay $\mu^+ \to e^+e^-e^+$ in one of 10^{15} muon decays. Upgrades to increase the intensities of the existing muon beams and the installation of a new beamline are currently under discussion at PSI. Upgrades providing muon intensities in excess of 10^9 muons per second are required to reach the aimed sensitivity of $\mathrm{B}(\mu^+ \to e^+e^-e^+) \sim 10^{-16}$.

The proposed experiment is highly complementary to other LFV searches for physics beyond the standard model, i.e. direct searches performed at the Large Hadron Collider (LHC) and indirected searches in the decay of taus and muons, such as the decay $\mu^+ \to e^+\gamma$, which is the subject of the *MEG* experiment currently in operation at PSI. The proposed experiment for the search $\mu^+ \to e^+e^-e^+$ will test lepton flavour violating models of physics beyond the Standard Model with unprecedented sensitivity.

This sensitivity is experimentally achieved by a novel experimental design exploiting silicon pixel detectors based on High Voltage Monolithic Active Pixel Sensors (HV-MAPS). This technology provides high granularity, important for precision tracking and vertexing, and allows one to significantly reduce the material budget by thinning down the sensors and by integrating the hit digitisation and readout circuitry in the sensor itself. The time information of the decay electrons[1], obtained from the pixel detector is further improved by a time-of-flight system consisting of a scintillating fiber hodoscope and tiles with Silicon Photo-Multipliers (SiPM) for light detection. By combining both detector systems accidental background can be reduced to reach the aimed sensitivity of $\mathrm{B}(\mu^+ \to e^+e^-e^+) \sim 10^{-16}$.

After testing of the first detector prototypes, that might commence in 2012-2013, the experiment could be performed in two phases. In the first phase (2014-2017) an existing muon beamline would provide a sensitivity of about $\mathrm{B}(\mu^+ \to e^+e^-e^+) \sim 10^{-15}$. In the second phase, the experiment will reach the ultimate sensitivity by exploiting a possible upgraded muon beamline after 2017 with an intensity of $2 \cdot 10^9$ muons per second. In absence of a signal LFV muon decays can then be excluded for $\mathrm{B}(\mu^+ \to e^+e^-e^+) < 10^{-16}$ at 90% confidence level.

[1]Here and in the following, the term "electron" denotes generically both decay electrons and positrons.

1 Motivation

In the Standard Model (SM) of elementary particle physics, the number of leptons of each family (lepton flavour) is conserved at tree level. In the neutrino sector, lepton flavour violation (LFV) has however been observed in the form of neutrino mixing by the Super-Kamiokande [1], SNO [2], KamLAND [3] and subsequent experiments. Consequently, lepton flavour symmetry is a broken symmetry, the standard model has to be adapted to incorporate massive neutrinos and lepton flavour violation is also expected in the charged lepton sector. The exact mechanism and size of LFV being unknown, its study is of large interest, as it is linked to neutrino mass generation, CP violation and new physics beyond the SM.

In the SM, charged lepton flavour violating reactions are forbidden at tree level and can only be induced by lepton mixing through higher order loop diagrams. However, the neutrino mixing loop diagram, see Fig. 1 a) is strongly suppressed in the SM with B $< 10^{-50}$ in muon decays and thus giving potentially high sensitivity to LFV reactions in models beyond the SM. Furthermore, LFV effects from new particles at the TeV scale are naturally generated in many models and are therefore considered to be a prominent signature for new physics. Fig. 1 b) shows an example where supersymmetric (SUSY) particles run in the loop.

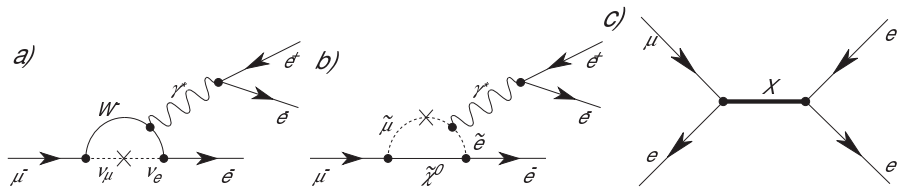

Figure 1: a) Feynman diagram for the $\mu \to eee$ process via neutrino mixing (indicated by the cross). b) Diagram for lepton flavour violation involving supersymmetric particles. c) Diagram for lepton flavour violation at tree level.

In many extensions of the SM, such as grand unified models [4–6], supersymmetric models [7] (see Fig. 1 b), left-right symmetric models [8–10], models with an extended Higgs sector [11] and models where electroweak symmetry is broken dynamically [12], an experimentally accessible amount of LFV is predicted in a large region of the parameters space. The observation of LFV in the charged lepton sector would be a sign for new physics, possibly at scales far beyond the reach of direct observation at e.g. the large hadron collider (LHC).

Beyond the Standard Model (BSM) lepton flavor violation can also be mediated by tree couplings as shown in Fig. 1 (c). These couplings could be mediated by new particles, like Higgs particles or doubly charged Higgs particles, R-parity violating scalar neutrinos or new heavy vector bosons which are for example motivated by models with extra dimensions [13, 14]. In contrast to the purely leptonic LFV processes, which are best tested in muon or tau decays, these models also predict semihadronic decays of tau leptons or the muon conversion process $\mu q \to eq'$, which is experimentally best tested in muon capture experiments.

Several experiments have been performed or are in operation to search for

Decay channel	Experiment	Branching ratio limit	Reference
$\mu \to e\gamma$	*MEGA*	$< 1.2 \cdot 10^{-11}$	[15]
	MEG	$< 2.4 \cdot 10^{-12}$	[18]
$\mu \to eee$	*SINDRUM*	$< 1.0 \cdot 10^{-12}$	[19]
$\mu\, Au \to e\, Au$	*SINDRUM II*	$< 7 \cdot 10^{-13}$	[20]

Table 1: Experimental limits on LFV muon decays

LFV in the decays of muons or taus. Most prominent are the search for the radiative muon decay $\mu \to e\gamma$ [15–18], the decay $\mu \to eee$ [19], the conversion of captured muons to electrons [20] and LFV tau decays [21–34].

The recent search performed by the *MEG*-Collaboration yields $\mathrm{B}(\mu \to e\gamma) < 2.4 \cdot 10^{-12}$ [18] and sets currently the most stringent limit on many LFV models. The *MEG* collaboration plans to continue operation until the end of 2012 in order to increase the number of stopped muons and to reach a sensitivity of a few times 10^{-13}. Plans to upgrade the experiment to further improve the sensitivity are under discussion.

In the near future the *DeeMe* experiment at J-PARC plans to improve the current muon-to-electron conversion limit of $\mathrm{B}(\mu\, Au \to e\, Au) < 7 \cdot 10^{-13}$ [20] by almost two orders of magnitude. By the end of the decade this limit could be improved by even four orders of magnitude by *COMET* at J-PARC and *Mu2e* at Fermilab.

Selected limits for lepton flavour violating muon decays and muon-to-electron conversion experiments are shown in Table 1.

2 Theory

The lepton flavor violating three electron decay of the muon can be mediated either via virtual loops or via tree diagrams. The most general Lagrangian for this decay can be written as [35]:

$$\begin{aligned} L_{\mu\to eee} \quad = \quad & \frac{4G_F}{2}\,[m_\mu A_R\, \overline{\mu_R}\sigma^{\mu\nu} e_L F_{\mu\nu} + m_\mu A_L\, \overline{\mu_L}\sigma^{\mu\nu} e_R F_{\mu\nu} \\ & + g_1\, (\overline{\mu_R} e_L)\, (\overline{e_R} e_L) + g_2\, (\overline{\mu_L} e_R)\, (\overline{e_L} e_R) \\ & + g_3\, (\overline{\mu_R}\gamma^\mu e_R)\, (\overline{e_R}\gamma_\mu e_R) + g_4\, (\overline{\mu_L}\gamma^\mu e_L)\, (\overline{e_L}\gamma_\mu e_L) \\ & + g_5\, (\overline{\mu_R}\gamma^\mu e_R)\, (\overline{e_L}\gamma_\mu e_L) + g_6\, (\overline{\mu_L}\gamma^\mu e_L)\, (\overline{e_R}\gamma_\mu e_R) \;+\; H.c.\,] \end{aligned} \tag{1}$$

The couplings of the radiative process, see penguin diagrams in Fig. 1 a) and b), are of tensor type (dipole couplings) and are described by the $A_{R,L}$ terms. Using the contact interaction formalism, the four fermion couplings of the tree diagram processes are described by scalar-type ($g_{1,2}$) and vector-type ($g_3 - g_6$) couplings. This ansatz is motivated by the high mass of the intermediate particle (see Fig. 1 c).

Off shell photon form factors, which can not be tested in $\mu \to e\gamma$ decays, also contribute to the terms g_3 - g_6. The contributions to the different LFV couplings depend on the model under consideration.

In case of non-zero dipole and four-fermion couplings also interference effects have to be considered, which can be exploited to investigate violation of time reversal (T-invariance).

By neglecting higher order terms in m_e, the total branching ratio of the decay can be expressed by:

$$\begin{aligned} \mathrm{B}(\mu \to eee) &= \frac{g_1^2 + g_2^2}{8} + 2\,(g_3^2 + g_4^2) \;+\; g_5^2 + g_6^2 \;+\; 32\, eA^2\, (\ln \frac{m_\mu^2}{m_e^2} - 11/4) \\ &+ \;\; 16\,\eta\, eA\, \sqrt{g_3^2 + g_4^2} + 8\,\eta'\, eA\, \sqrt{g_5^2 + g_5^2} \quad , \end{aligned} \tag{2}$$

where the definition $A^2 = A_L^2 + A_R^2$ is used. The pure photonic loop contribution (term including A^2) is logarithmically enhanced compared to the other contact interaction or interference terms. The constants η and η' are T-violating mixing parameters. In case of a signal the different terms can be measured from the angular distribution of $\mu \to eee$ decay particles using a polarized muon beam.

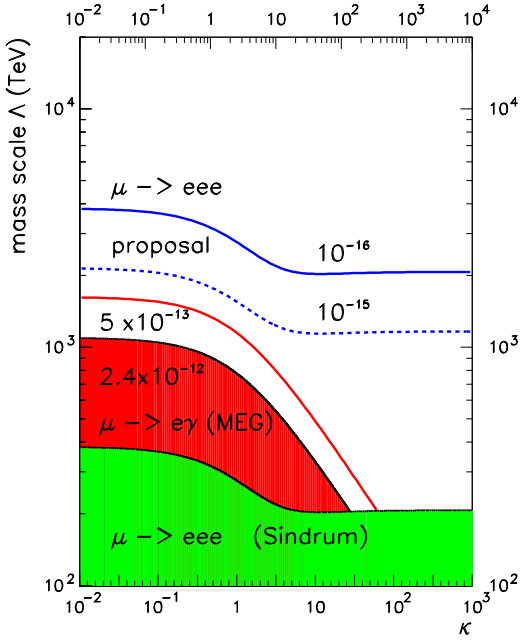

Figure 2: Experimental limits and projected limits on the LFV mass scale Λ as a function of the parameter κ (see equation 3).

To compare the new physics mass scale reach of the photonic and non-photonic LFV coupling and to allow comparisons between the decays $\mu \to e\gamma$ and $\mu \to eee$ the following simplified Lagrangian is assumed:

$$L_{LFV} = \frac{m_\mu}{(\kappa+1)\Lambda^2}\, \overline{\mu_R} \sigma^{\mu\nu} e_L F_{\mu\nu} \;+\; \frac{\kappa}{(\kappa+1)\Lambda^2}\, (\overline{\mu_L}\gamma^\mu e_L)\, (\overline{e_L}\gamma_\mu e_L) \quad , \tag{3}$$

where for the contact interaction (right) term exemplarily the left-left vector coupling is chosen. In this definition a common mass scale Λ is introduced and the parameter κ describes the ratio of the contact interaction term amplitude over the amplitude of the loop contribution. Limits on the mass scale Λ as

obtained from the experimental bounds on $\mathrm{B}(\mu \to e\gamma) < 2.4 \cdot 10^{-12}$ (90% CL *MEG* 2011) and $\mathrm{B}(\mu \to eee) < 1.0 \cdot 10^{-12}$ (90% CL *SINDRUM*) are shown in Fig. 2 as function of the parameter κ. The process $\mu \to e\gamma$ constrains the mass scale at low values of κ (dipole coupling) whereas for $\kappa \gtrsim 10$ the $\mu \to eee$ is constraining the four fermion contact interaction region. For comparison also projected sensitivities are shown of the *MEG* experiment for $5 \cdot 10^{-13}$ and of the proposed $\mu \to eee$ experiment for sensitivities of 10^{-15} (phase I) and 10^{-16} (phase II). It can be seen that for $\mathrm{B}(\mu \to eee) \lesssim 10^{-15}$ LFV processes are best constrained by the proposed $\mu \to eee$ experiment for all values of κ in this comparison.

In case of dominating tensor couplings ($A \neq 0$) a quasi model independent relation between the $\mu \to eee$ decay rate and the $\mu \to e\gamma$ decay rate can be derived (limit $\kappa \to 0$):

$$\frac{\mathrm{B}(\mu \to eee)}{\mathrm{B}(\mu \to e\gamma)} \approx 0.006 \tag{4}$$

This ratio applies e.g. for many supersymmetric models, where LFV effects are predominantly mediated by gauge bosons running in the loop.

In order to set competitive constraints on LFV dipole couplings a limit on the branching ratio of the decay $\mu \to eee$ needs to be about two orders of magnitude smaller than for the decay $\mu \to e\gamma$.

The non-observation of LFV of charged leptons in past and present experiments might at a first glance be surprising, as the mixing angles in the neutrino matrix have been measured to be large (maximal). This huge suppression of LFV effects is however accidental and due to the fact that (a) neutrinos are so much lighter than charged leptons and (b) the mass differences between neutrinos (more precisely the square of the mass differences) are very small compared to the W-boson mass. The situation completely changes if new particles beyond the SM model are introduced. If e.g. SUSY is realized at the electroweak scale, the scalar partners of the charged leptons (sleptons) will have large masses, and if not fully degenerate, induce LFV interactions via loop corrections. This argument applies for many models, which predict new particles coupling to leptons.

Seesaw and Left-Right symmetric (supersymmetric) models are good candidates for realizing grand unification, which also unify quark and lepton mass matrices. Moreover, it has been shown that LFV effects in the low energy limit can be related to mixing parameters at the GUT scale or to heavy Majorana masses in these models [36, 37]. Seesaw models are very attractive as they are also able to naturally explain the smallness of the masses of the left handed neutrinos.

New heavy particles as predicted e.g. by Little Higgs models, Higgs Triplet models or models with extra dimensions can also induce sizable LFV effects. In the following, selected models are discussed in the context of the proposed experiment.

2.1 SUSY Models

Despite the fact that the most simple supersymmetric models with light squarks and gluinos were recently excluded by LHC experiments [38–41], supersymmetry can still exist in nature, just at higher mass scales or in more complex realisations.

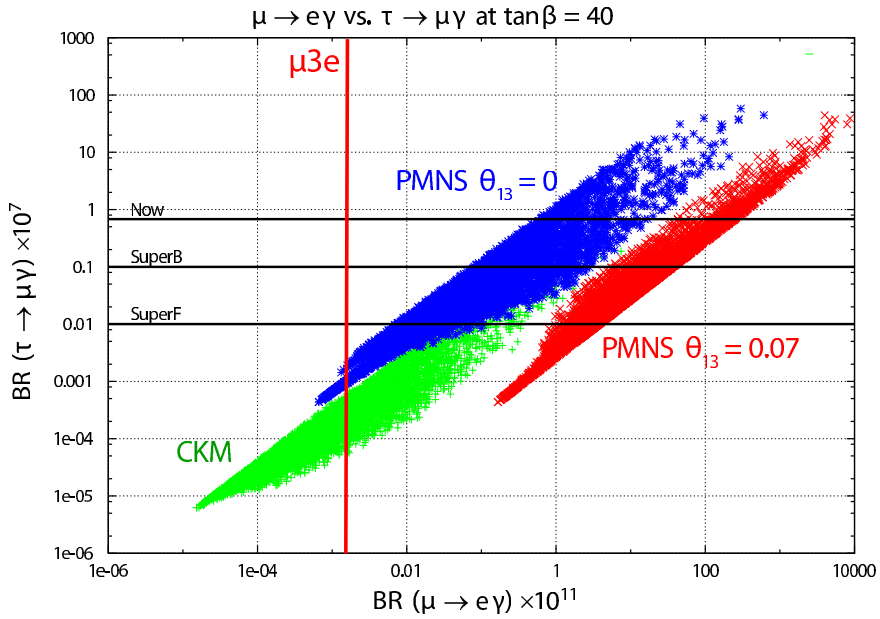

Figure 3: Radiative branching ratios $\mu \to e\gamma$ vs. $\tau \to \mu\gamma$ from a SUSY-GUT model parameter scan for $\tan\beta = 40$ [36]. The different colors represent different flavor mass matrices at the GUT scale. The corresponding $\mu \to eee$ branching ratio is given by $0.006 \times \mathrm{B}(\mu \to e\gamma)$. The envisaged sensitivity of 10^{-16} for $\mathrm{B}(\mu \to eee)$ corresponds here to $\sim 1.5 \cdot 10^{-14}$ for $\mathrm{B}(\mu \to e\gamma)$. In addition, sensitivities of current and future B-factories for the complementary LFV tau decay $\tau \to \mu\gamma$ are shown.

Lepton Flavor Violation in the framework of SUSY-GUT models was discussed in [36] for two different realisations of the flavor matrix at the GUT scale. The "CKM-type" parameterisation has CKM-like fermion mixing angles at the GUT scale whereas the "PMNS-type" parameterisation has neutrino like mixing angles (bi-maximal mixing) with θ_{13} being a free parameter. In Fig. 3 the branching ratios for the LFV radiative decays of the tau and the muon is shown for a Higgs Doublet expectation value ratio of $\tan\beta = 40$. It can be seen that the PMNS scenario can be almost completely ruled out independent of the value of θ_{13} for $\mathrm{B}(\mu \to e\gamma) < 10^{-14}$, which corresponds to the aimed sensitivity of the $\mu \to eee$ search with $\mathrm{B}(\mu \to eee) < 10^{-16}$ using equation 4. The figure also shows the complementarity to LFV searches using taus in the process $\tau \to \mu\gamma$. All parameter sets which might be tested in future B-factories might be completely ruled out by the proposed experiment.

The sensitivity of the decay $\mu \to eee$ on the small neutrino mixing angle θ_{13} was studied in [37]. Although basically all therein investigated SUSY parameter sets [42] were recently excluded by the LHC experiments it was generally shown that the LFV branching ratio is largely reduced for small neutrino mixing angles θ_{13} . Thus high experimental sensitivity would be required in case of very small angles $\theta_{13} < 1°$.

This theoretical result is of special interest as recent neutrino oscillation measurements seem to indicate a non-vanishing and not too small angle θ_{13} [43–46]. Currently the most accurate measurement is provided by the *Double Chooz* reactor neutrino experiment [46] yielding $\sin\theta_{13}^2 = 0.085 \pm 0.029(\text{stat}) \pm 0.042(\text{syst})$. Furthermore, a combined analysis [47] of the accelerator and reactor data from *T2K*, *MINOS* and *Double Chooz* sets even tighter constraints and gives 3.4 sigma evidence for a non-zero angle θ_{13}. These preliminary results are encouraging as large values of $\sin\theta_{13}^2$ lead potentially to large LFV effect in many BSM models.

Both studies [36, 37] were also discussing specific SUSY-GUT models, which are able to generate the observed amount of baryon asymmetry (e.g. leptogenesis) as observed in the universe in the context of LFV. The Searches for $\mu \to eee$ will also add important information to these class of models.

The complementarity of the $\mu \to eee$ and $\mu \to e\gamma$ searches in the context of SO(10) SUSY was discussed in [48]. It is shown that the ratio $\text{B}(\mu \to eee)/\text{B}(\mu \to e\gamma)$ is typically α_{em} for SO(10) SUSY models whereas the ratio can be of the order of one, or even higher in SU(5) type SUSY models due to possible cancellations of the radiative $\mu \to e\gamma$ loops.

2.2 Non-SUSY Models

Little Higgs Models with T-parity (LHT) also enhance the $\mu \to eee$ decay and predict $\text{B}(\mu \to eee)/\text{B}(\mu \to e\gamma) \approx 0.02 - 1$. The reason is that photon penguins, which typically dominate in Minimal Supersymmetric Models and contribute to the dipole form-factor, are replaced by Z^0 penguin and box diagrams in LHT models. These additional contributions enhance the $\mu \to eee$ decay process [49, 50].

In Left-Right Symmetric models, new heavy Higgs triplets are predicted, which mediate LFV via loops and tree diagrams. In [11] these LFV violating effects are studied in a model where the triplet Higgs is responsible for neutrino mass generation. Fig. 4 shows the predicted branching ratios for each of the three LFV muon decays and for different realisations of the neutrino mass hierarchy. For the hierarchical case, Fig. 4 b), the branching ratios are expected to be of similar size whereas for the degenerate, Fig. 4 a), and the inverted case, Fig. 4 c), the $\mu \to eee$ branching ratio dominates. As the LFV-mediating Higgs triplet boson does not couple to quarks, the $\mu \to eee$ decay is enhanced compared to the $\mu \to e\gamma$ decay and the muon-to-electron conversion processes, which are both loop suppressed.

Enhancement of the LFV tree diagrams tested in $\mu \to eee$ is found to be large also in extra dimension models [13, 51] or models with new heavy Z bosons. In Randall-Sundrum (RS) models [13], flavor changing neutral currents (FCNCs) arise already at the tree level. This is caused by the flavor-dependent couplings of these gauge bosons, due to their non-trivial profiles in the extra dimension. Moreover, FCNCs arise through the exchange of the Higgs boson, as due to the contribution to the fermion masses from compactification, there is a misalignment between the masses and the Yukawa couplings.

Electroweak precision observables suggest that for RS models featuring the Standard Model gauge group, the new-physics mass scale M_{KK} (the scale of the Kaluza Klein excitations) should not be lower than $\mathcal{O}(10\,\text{TeV})$ at 99% CL [52–54]. Thus, without additional structure/symmetries, the experimental situation

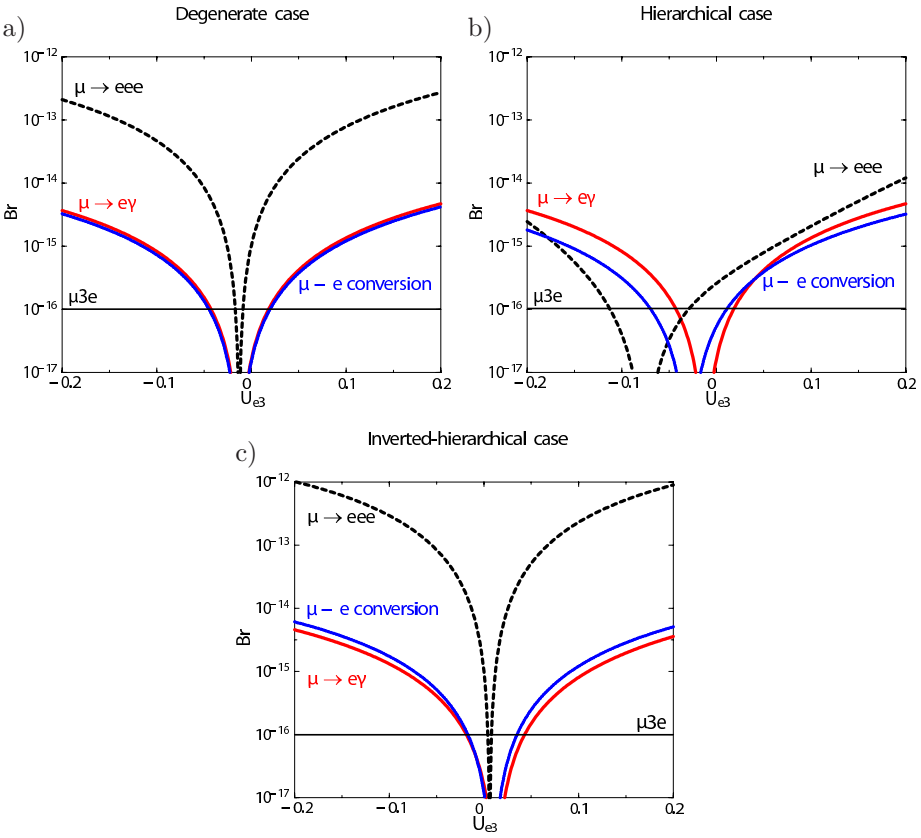

Figure 4: Branching ratios of B($\mu \to eee$), B($\mu \to e\gamma$) and muon conversion B($\mu \to e$) in different Higgs triplet scenarios with a degenerated, hierarchical or inverted mass hierarchy of the neutrinos as function of the neutrino mixing matrix element U_{e3}. These plots were taken from [11].

suggests that it could be challenging to find direct signals from RS models at the LHC. In such a situation, precision experiments, like the measurement of the decay $\mu \to eee$, will furnish the only possibility to see the impact of warped extra dimensions.

2.3 Theory Summary

The search for the decay $\mu \to eee$ is in itself of fundamental interest and might reveal surprises not foreseen by any of the models discussed above. This search is largely complementary to other LFV searches, in particular to the decay $\mu \to e\gamma$ and to the $\mu \to e$ conversion in muon capture experiments. In a wide range of models for physics beyond the standard model, the highest sensitivity in terms of branching ratio is expected for the $\mu \to eee$ decay process.

3 Experimental Situation

3.1 *SINDRUM* Experiment

The *SINDRUM* experiment was in operation at PSI from 1983-86 to search for the process $\mu \to eee$. No signal was found and the limit $\mathrm{B}(\mu \to eee < 10^{-12})$ was set at 90% CL [19], assuming a decay model with a constant matrix element.

The main components of the experiment were a hollow double-cone shaped target of dimension 58 mm×220 mm to stop surface muons of 28 MeV/c in a solenoidal magnetic field of 0.33 Tesla, five layers of multiwire proportional chambers and a trigger hodoscope. The main tracking parameters which were most relevant for the search sensitivity of the experiment are shown in Table 2.

The time resolution obtained by the hodoscope of less than 1 ns was, together with the achieved momentum resolution, sufficient to suppress the accidental background completely.

After all selection cuts, no candidate event was seen by the *SINDRUM* experiment. The sensitivity of the experiment was mainly determined by the $\mu \to eee\nu\nu$ background process and estimated as $5 \cdot 10^{-14}$ [55]; the obtained limit was basically given by the limited number of muon stops.

SINDRUM parameter	Value	
rel. momentum resolution σ_p/p	5.1%	($p = 50$ MeV/c)
rel. momentum resolution σ_p/p	3.6%	($p = 20$ MeV/c)
polar angle σ_θ	28 mrad	($p = 20$ MeV/c)
vertex resolution σ_{dca}	≈ 1 mm	
MWPC layer radiation length in X_0	0.08% - 0.17%	

Table 2: *SINDRUM* tracking parameter taken from [19].

3.2 *MEG* Experiment

The *MEG* experiment at PSI is in operation since 2008 and is searching for the LFV decay $\mu \to e\gamma$. The main components used for event reconstruction are drift chambers for positron detection and a liquid xenon calorimeter for photon detection.

In the first running period in the year 2008 about 10^{14} muons were stopped on target [17]. No signal was found and a limit on the decay of $\mathrm{B}(\mu \to e\gamma) < 2.8 \times 10^{-11}$ (90% C.L.) was set.

After upgrading the detector the search sensitivity and the limit was improved using data taken in the years 2009/2010 to $\mathrm{B}(\mu \to e\gamma) < 2.4 \times 10^{-12}$ (90% C.L.) [18].

The dominant background contribution for $\mu \to e\gamma$ comes from accidentals where a high energy photon from a radiative muon decay or from a bremsstrahlung process is recorded, overlayed with a positron from the upper edge of the Michel spectrum. This accidental background mainly determines the final sensitivity of the experiment.

The amount of background is predominantly determined by the timing, tracking and energy resolution. Selected resolution parameters as achieved in

the 2009 run are summarized in Table 3. The *MEG* experiment will continue operation until the end of 2012. The final sensitivity is expected to be a few times 10^{-13}. The *MEG* experiment has started to discuss possible upgrades to further improve the sensitivity. These numbers are to be compared to the bound from the earlier *MEGA* experiment of $\mathrm{B}(\mu \to e\gamma) < 1.2 \times 10^{-11}$ [15].

MEG parameter 2011 publ.	Value
rel. momentum resolution σ_p/p	0.7% (core)
polar angle σ_θ	9 mrad
azimuthal angle σ_ϕ	7 mrad
radial vertex resolution σ_R	1.1 mm
long. vertex resolution : σ_Z	1.5 mm

Table 3: Best *MEG* tracking parameter resolutions achieved in the year 2009/2010. The resolutions are given for positrons of 53 MeV/c momentum. Values taken from [18].

The study of the $\mu \to e\gamma$ decay sets stringent bounds on models predicting new heavy particles mediating LFV dipole couplings. These dipole couplings can also be tested in the process $\mu \to eee$, where the sensitivity is reduced by a factor of $\frac{\alpha}{3\pi}(\ln(m_\mu^2/m_e^2) - 11/4) = 0.006$. The projected sensitivity of 10^{-13} of the *MEG* experiment corresponds accordingly to a sensitivity of about 10^{-15} in the search for the $\mu \to eee$ decay and the envisaged sensitivity of $\mathrm{B}(\mu \to eee) = 10^{-16}$ corresponds to more than one order of magnitude higher sensitivity compared to the *MEG* experiment.

The *MEG* experiment, in contrast to the proposed $\mu \to eee$ experiment, has no sensitivity to lepton flavor violating four-fermion contact interaction couplings.

3.3 Muon Conversion Experiments

Muon to electron conversion experiments $\mu \to e$ on nuclei exploit the clear signature of monochromatic electrons. Differently to the search for LFV muon decays, which are performed using DC anti-muon beams in order to reduce accidental backgrounds, muon conversion experiments are performed using pulsed muon beams in order to reduce the rapidly decaying pion background. A limitation of this type of experiment is the background from ordinary decays of captured muons with large nuclear recoil and from pions.

The most stringent limits for muon-electron conversion on various nuclei have been obtained by the *Sindrum II* collaboration [20, 56, 57]. The strongest limit has been set using a gold target $\mathrm{B}(\mu\, Au \to e\, Au) < 7 \cdot 10^{-13}$ [20].

Similar to the $\mu \to eee$ process, the sensitivity to dipole couplings in muon conversion is reduced by about α_{em} compared to the more direct $\mu \to e\gamma$ search. However, new experiments planned at Fermilab (*Mu2e* [58, 59]) and at J-PARC (*COMET* [60, 61] and *PRISM* [62, 63]) aim for branching ratios of 10^{-16} or smaller relative to the captured muon decay and have a higher sensitivity to LFV dipole couplings than the running *MEG* experiment. Similar to the $\mu \to eee$ process, also four-fermion couplings are tested in $\mu \to e$ conversion experiments.

These couplings involve light quarks and are thus complementary to all other LFV search experiments.

The *Mu2e* and *COMET*-experiments are ambitious projects and are expected to come into operation at earliest by the end of this decade. In a few years time the *DeeMe* experiment at J-PARC will come into operation, aiming for a sensitivity for muon-to-electron conversions of 10^{-14}.

3.4 LFV at the Large Hadron Collider

LFV signatures might be observed at the LHC if e.g. supersymmetric particles are discovered, which naturally generate LFV couplings in slepton mass mixing. Consequently, if sleptons are light enough to be produced in pairs, different lepton flavors might show up in decay chains such as: $\tilde{\ell}^+\tilde{\ell}^- \to \ell^+\ell^{-\prime}\chi^0\chi^0$.

New scalar or vector particles could also have lepton violating tree couplings and might be directly reconstructed from resonance peaks: $H,\ Z' \to \ell\ell'$. Due to the existing bounds on flavor changing processes, these LFV decays are small and difficult to detect above the large background from WW-production with subsequent leptonic decays.

If new particles exist at the TeV mass scale, i.e. in the discovery reach of the LHC, it is very likely that precision experiments will discover lepton flavor violation via radiative loops. Dedicated LFV search experiments like the proposed $\mu \to eee$ experiment would then allow one to measure the LFV couplings of the new particles, complementary to the TeV scale experiments at the LHC.

Conversely, in the case that no new physics (excluding the SM Higgs boson) were discovered at the LHC, the discovery of LFV in precision experiments is not excluded as e.g. rare muon decays are testing the mass scale > 1 PeV, three orders of magnitude higher than at LHC.

4 The Decay $\mu \to eee$

4.1 Kinematics

The decay $\mu \to eee$ proceeds promptly. For discriminating signal and background, energy and momentum conservation can be exploited. The vectorial sum of all decay particle momenta should vanish:

$$|\vec{p_{tot}}| \;=\; |\sum \vec{p_i}| \;=\; 0 \tag{5}$$

and the total energy has to be equal to the muon mass.

The energies of the decay electrons (positrons) are in the range $0 - 53$ MeV. All decay particles must lie in a plane and the decay is described by two independent variables in addition to three global rotation angles, which describe the orientation in space.

4.2 Detector Acceptance

The acceptance of the proposed $\mu \to eee$ experiment is determined by its geometrical acceptance and energy coverage. For various coupling assumptions about the LFV amplitude, see also equation 1, the energy spectrum of the highest energy, E_1, and lowest energy decay particles, E^e_{min}, are shown in Figures 5 and 6, respectively. In order to achieve a high acceptance, the detector must be able to reconstruct tracks with momenta ranging from half the muon mass down to a few MeV with large solid angle coverage. The proposed experiment should cover the energy range > 10 MeV to provide acceptances of 50% or more for all models.

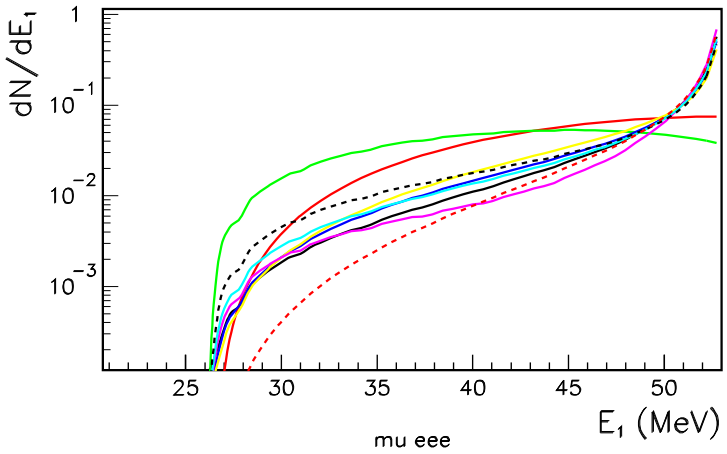

Figure 5: Energy distribution of the highest energy positron in the decay $\mu^+ \to e^+e^-e^+$ for different effective LFV models. The solid red and the green lines correspond to pure four-fermion contact interaction models (no penguin) contribution.

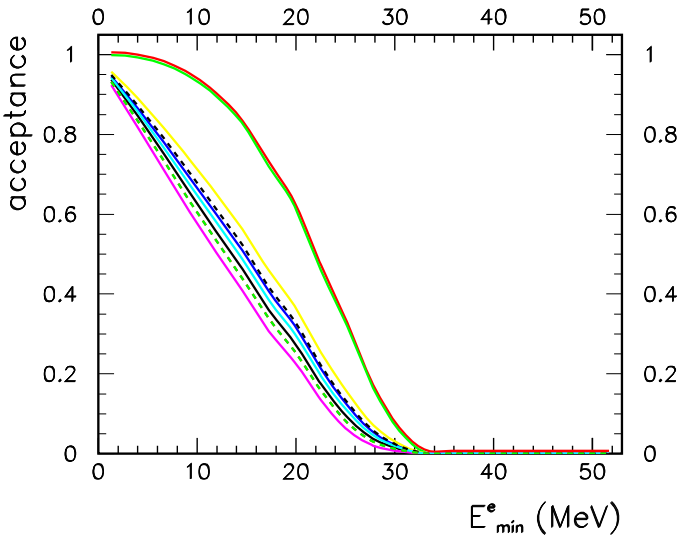

Figure 6: Acceptance of the lowest energy decay electron (positron) for different effective LFV models as function of the minimum transverse momentum. The solid red and green lines correspond to pure four-fermion contact interaction models (no penguin) contribution.

4.3 Backgrounds

The final sensitivity of the proposed experiment depends on the ability to reduce backgrounds from various sources. Two categories of backgrounds are considered; accidental backgrounds that scale with the square of the beam intensity and irreducible backgrounds, such as $\mu^+ \to e^+e^+e^-\nu\nu$, which strongly depend on the granularity and resolution of the detector.

Using a beam of positive muons, one of the main processes contributing to accidental background is that of the ordinary Michel decay $\mu^+ \to e^+\nu\nu$. This process does not produce a negatively charged particle (electron), which is one of the main characteristics of the $\mu^+ \to e^+e^+e^-$ decay, and can therefore only contribute as potential background if a track is wrongly reconstructed. Other processes which "naturally" provide negatively charged tracks (electrons) are radiative decays with internal or external photon conversions or Bhabha scattering.

In the following sections the main background sources considered are discussed.

4.3.1 Radiative Muon Decays

The process $\mu^+ \to e^+\gamma\nu\nu$ (branching fraction $1.4{\cdot}10^{-2}$ for photon energies above 10 MeV [64]) can deliver an oppositely charged electron if the photon converts either in the target region or in the detector. Contributions from conversions outside of the target are greatly suppressed if a vertex constraint is applied or

by minimising the material in both the target and detector. Photon conversions in the target generates an event topology similar to the radiative decay with internal conversion: $\mu \to eee\nu\nu$, which is discussed below.

Due to the missing energy from the neutrinos, this process mainly contributes to the accidental background in combination with an ordinary muon decay.

4.3.2 Internal Conversions

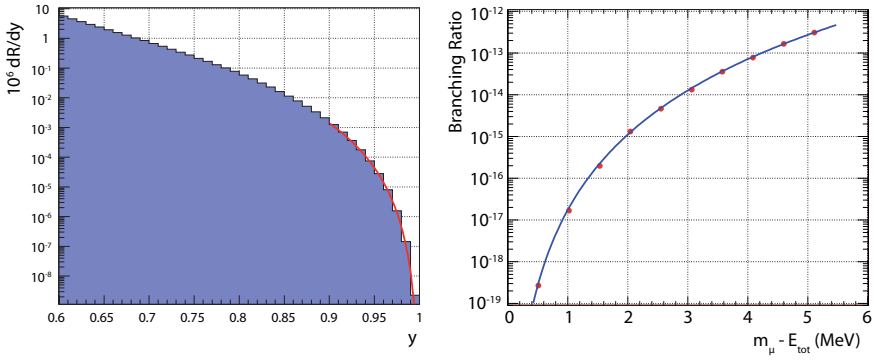

Figure 7: Summed energy of the charged leptons normalised to the muons mass, y, in the decay $\mu \to eee\nu\nu$ (left) and branching ratio of the same process as a function of the missing energy $m_\mu - E_{tot}$ cut (right). Figures adapted from [65].

The decay $\mu \to eee\nu\nu$ occurs with a branching fraction of $3.4 \cdot 10^{-5}$ [64]. It can be distinguished from the $\mu \to eee$ process by making use of energy and momentum conservation to reconstruct the undetected neutrinos; in order to separate the $\mu \to eee$ events from $\mu \to eee\nu\nu$ events, the total momentum in the event is required to be zero and the energy equal to the muon rest energy. The energy spectrum and the branching fraction as a function of the energy cut of the $\mu \to eee\nu\nu$ process [65] are shown in Fig. 7. This process is the most serious background for the $\mu \to eee$ search and can only be resolved by a very good energy resolution.

4.3.3 Bhabha Scattering

Positrons from the ordinary muon decay or beam-positrons can undergo Bhabha scattering with electrons in the target material, leading to an electron-positron pair from a common vertex. Due to the missing energy this process mainly contributes to the accidental background in combination with an ordinary muon decay.

4.3.4 Pion decays

Certain decays of pions, especially $\pi \to eee\nu$ (branching fraction $3.2 \cdot 10^{-9}$ [64]) and $\pi \to \mu\gamma\nu$ (branching fraction $2.0 \cdot 10^{-4}$ [64]) with subsequent photon conversion are indistinguishable from signal events if the momenta of the final state particles fit the muon mass hypothesis; a low pion contamination of the

primary beam, the small branching fraction and the small slice of the momentum is assumed to lead to negligible rates in the kinematic region of interest.

4.3.5 Summary of Background Sources

First simulation studies have been performed to calculate the different background contributions. First results indicate that purely accidental backgrounds for $\sim 10^9$ muons stops per second are negligible for the proposed high resolution detector. The main concern are irreducible backgrounds, such as the process $\mu \to eee\nu\nu$, which can only be reduced by a very good tracking resolution resulting in total energy resolution of $\sigma_E < 1$ MeV for the aimed sensitivities $< 10^{-15}$.

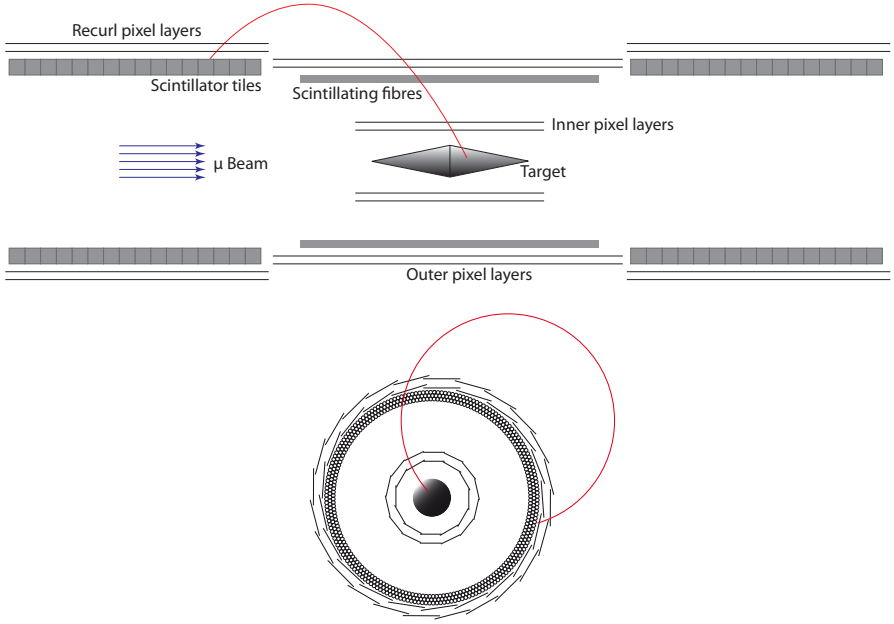

Figure 8: Schematic view of the proposed experiment for the search of $\mu \to eee$ (not to scale). Shown are the detector components in the side view (top) and in the transverse plane (bottom).

5 A Novel Experiment Searching for $\mu \to$ eee

The proposed experiment aims for a sensitivity of $\mathrm{B}(\mu^+ \to e^+e^-e^+) < 10^{-16}$ (10^{-15}) at 90% CL for a beam intensity of $2{\cdot}10^9$ ($2{\cdot}10^8$) muon stops per second. Reaching this sensitivity requires a large geometrical coverage and suppression of any possible background to a level below 10^{-16}.

The most serious backgrounds are considered to be the radiative muon decay $\mu^+ \to e^+e^-e^+\bar{\nu}_\mu\nu_e$ with a branching fraction of $3.4 \cdot 10^{-5}$ and accidentals, which must be efficiently suppressed by an excellent vertex and timing resolution of the detector. Suppression of backgrounds requires a precise measurement of the electron and positron momenta in order to reconstruct the kinematics. By exploiting kinematical constraints accidental backgrounds can be further reduced and missing momentum and energy due to the additional neutrinos in the $\mu^+ \to e^+e^-e^+\bar{\nu}_\mu\nu_e$ process can be detected. The kinematic reconstruction of candidate events is mainly deteriorated by multiple scattering of the low energy electrons. Therefore, the material budget of the target and detector, which must be operated in a helium atmosphere, has to be kept to a minimum.

In summary, a detector capable of precise momentum, vertex and timing reconstruction at very high rates is needed. We propose to construct an experiment with a long high precision tracker based on thin silicon pixel detectors and a system of time-of-flight hodoscopes, see Fig. 8, placed in a homogeneous solenoidal magnetic field of about $1-1.5$ Tesla. In the final sensitivity phase the experiment shall be performed at the highest intensity muon beamline available at PSI.

5.1 Muon Beam

A multi-staging approach is envisaged for the experiment, incorporating an initial experimental test-phase up to 2014, followed by an intermediate sensitivity-goal experiment of $B(\mu^+ \to e^+e^-e^+) \sim \mathcal{O}(10^{-15})$ from 2014-2017, requiring a muon stop-rate of about $2 \cdot 10^8$ Hz. Finally, post 2017, a full sensitivity-goal experiment aiming at $\mathcal{O}(10^{-16})$ with a required muon stopping rate of $2 \cdot 10^9$ Hz is planned.

5.1.1 Test Phase

For the initial test phase, a lower intensity secondary beam line, such as that of the PiE1 channel, could be used to produce either surface muons ("monochromatic" muons produced by stopped-pion decay at the surface of the primary production target) or positrons, for the realistic testing of sub-detectors and associated electronics.

5.1.2 Intermediate Sensitivity Experiment (Phase I)

The intermediate sensitivity experiment, requiring a stopped surface muon rate of $> 10^8$ Hz leaves only one choice of channel available at PSI, namely the PiE5 channel, one of the world's most intense surface muon beams, which is currently in use by the *MEG* experiment. If the *MEG* experiment is going to be continued beyond the year 2012, the channel could be shared between both experiments. In order to accommodate the *Mu3e* experiment in PiE5, without removing the COBRA magnet of the *MEG* experiment, the setup would have to be restricted to the front-part of the area (similar to the current shared layout of the *MEG* experiment with the Lamb-shift experiment). This would require a new compact beam line comprising of at least two dipole magnets and several quadrupole magnets in order to couple the PiE5 channel to the *Mu3e* magnet and using the *MEG* Wien-filter as a beam positron separator. Both, this scenario and the required intensity increase are still under study.

5.1.3 Final Sensitivity Experiment (Phase II)

The ultimate sensitivity goal beam, requiring muon intensities in excess of 10^9 Hz is also currently under study. A prime candidate to enable the achievement of this aim is derived from the idea of using the target window of the Swiss spallation neutron source (SINQ) for the production of an intense low-energy surface muon beam [66]. Initial muon flux estimates have been confirmed by means of realistic Monte-Carlo simulations and show that enhancement factors of two-to-three orders of magnitude might be possible if compared to the current primary target E situation and hence this would satisfy the intensity requirement for this phase of the experiment.

The large intensity enhancement, compared to the target E situation, would be 4-fold: the increased number of primary proton interactions, the increase in the pion production cross-sections for backward production angles, an increase in the pion production cross-sections due to the higher-Z materials of the spallation target and finally an increase due to the availability of the high-energy part of the cross-sections in producing "useful" pions that stop in the spallation target window.

The high intensity spallation source option would require a new beam line viewing the SINQ target window. One possible solution, which uses the existing upward incoming proton beam line to extract the muons, would simplify such a solution technically. This option however, could only be implemented in conjunction with a longer SINQ shutdown or planned target modification (possible in 2016).

5.2 Target

The goal of the target design is to uniformly stop, with high efficiency, muons in a large surface volume for good vertex separation, while keeping the amount of target material seen by the decay electrons at a minimum. The baseline design for the target is a thin ($\sim$ 60 µm) hollow aluminium double cone of 100 mm length and 20 mm diameter; a geometry similar to the one used by *SINDRUM*, see Fig. 8. Simulations using GEANT4 [67, 68] show that such a target will stop more than 90% of 28 MeV/c muons. Alternatively, kapton® (polyamide) or other low-Z materials could be used.

5.3 Magnet

A strong magnetic field of $B = 1 - 1.5$ T is needed to measure the momentum of tracks, with high precision, in a long cylindrical volume of about 2 m length and 1 m in diameter.

In a solenoidal magnetic field, recurling tracks produce a higher hit multiplicity in the tracker compared to other field configurations, for example magnets with a field gradient such as the COBRA magnet of *MEG*. Simulation studies have shown that recurling tracks and the increased hit multiplicity do not pose a severe problem for the track reconstruction. On the contrary it is found that the homogeneous solenoidal magnetic field greatly simplifies track reconstruction. In addition it provides an uniform momentum resolution.

5.4 Tracker Design

In order to reduce efficiently the background from muon decays with internal conversion, $\mu \to eee\nu\nu$, a very good momentum (energy) resolution of the tracker is of the highest importance. Therefore it is planned to use "thinned" ($30 - 50$ µm) silicon pixel detectors for high precision tracking. For small pixel sizes hit resolution effects can be neglected and the momentum resolution of the decay electrons is solely given by multiple scattering.

5.4.1 General Considerations

The track momentum resolution in a multiple scattering dominated environment depends mainly on the number of detector layers and their thickness. For equidistant spacing of the layers and not too large bending angles (linear approximation) the relative momentum resolution is given by [69]:

$$\frac{\sigma_p}{p} = \frac{N-1}{\sqrt{N-2}} \frac{b}{BL} \tag{6}$$

with N being the numbers of layers, B the strength of the magnetic field and L the effective length defined as distance between the first and last layer. The

parameter b describes the deflection in each layer and is related to the root mean square (RMS) of the multiple scattering angle:

$$\Phi_{RMS} \;=\; b/p \tag{7}$$

and can be calculated using [64]:

$$b \;=\; \sqrt{x/X_0} * (1 + \log(x/X_0)) \times 13.6 \text{ MeV} \quad . \tag{8}$$

As can be seen from eq. 6 the momentum resolution is degraded proportional with $\sqrt{N}$ for a large number of layers. For other geometries similar scaling laws can be derived. Therefore only a small number of tracking layers (3-4) should be chosen in a multiple scattering dominated environment for measuring particle momenta.

For precise momentum reconstruction a large lever arm of undisturbed track bending in the magnetic field is crucial. It can be shown that track momenta are extremely precisely measured in half-turns, i.e. the position of hits and the directions of the trajectory is measured before and after a half-turn bending.

For such a geometry the relative momentum resolution in the central region of the experiment can be approximated by:

$$\frac{\sigma_p}{p} \approx \frac{\Phi^2_{RMS}}{4} \quad , \tag{9}$$

and depends quadratically on the size of the multiple scattering. For the proposed experiment the root mean square of the multiple scattering angle is in the region of $\Phi_{RMS} = 2$ (10) mrad for particle momenta of $p = 50$ (10) MeV/c. Using recurling tracks the momentum resolution is about one order of magnitude better than for standard tracking techniques exploiting a single particle passage, where the bending angles between detector layers are significantly smaller, compare Fig. 8. Consequently, the design of the proposed experiment is therefore optimised to measure recurling tracks with high acceptance.

5.4.2 Tracker Design

The tracker consists of two cylinders of double pixel layers. Tracks are reconstructed by matching hit pairs from the inner two layers with hit pairs in the outer two layers. From the hit coordinates in the inner shorter double cylinder the direction of particles coming from the target region is derived. The hit coordinates, measured at the longer outer cylinder, are used to extrapolated the trajectory and to find the corresponding hit pair of the recurling track.

The acceptance of the experiment is increased by extending the outer cylinder with pixel sensors, so called recurl stations, which provide additional hit pairs to reconstruct precisely particles recurling in a downstream or upstream direction.

The design is completed by time-of-flight hodoscopes. A scintillating fiber hodoscope in the central region provides timing information for all particles, with a time resolution of about 1 ns. Scintillator tiles placed downstream and upstream provide additional and precise timing information for recurled tracks, with a resolution of about $0.1 - 0.2$ ns. Precision timing information will reduce the accidental background rate by about 2-3 orders of magnitude.

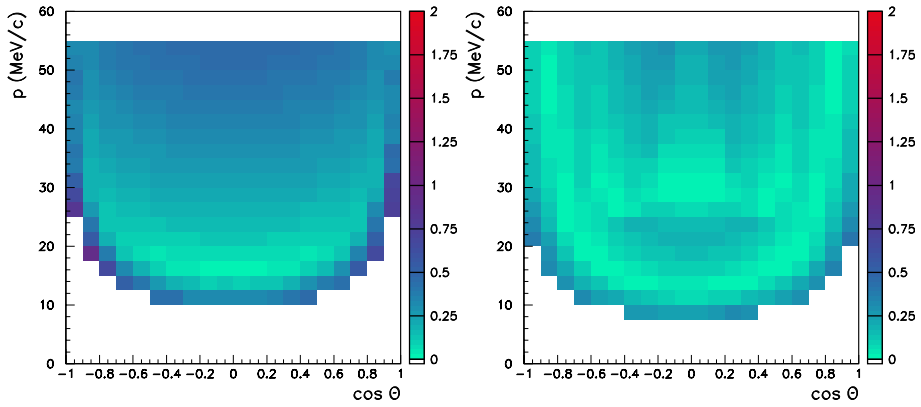

Figure 9: Momentum resolution of electrons as function of the momentum p and the polar angle $\cos\theta$ from multiple scattering alone, for the "two cylinder design" with radii 2.0 and 7.5 cm (left) and the "three cylinder design" with radii 2.0, 6.0 and 14 cm(right) using a magnetic field of $B = 1.0$ Tesla.

The momentum resolution of the experiment is basically determined by the recurling tracks alone and, in the proposed design, is not compromised by the additional timing counters, see Fig. 8. Another advantage of the proposed design is that most of the infrastructure, i.e. supports, cables, etc., are located outside the active volume of the experiment. Only the active structures like sensors and flex-prints contribute to the material budget.

The expected momentum resolution of this design, calculated considering multiple scattering only, is shown in Fig. 9 left. It can be seen the momentum resolution is everywhere better than 1 MeV/c, and in most regions of phase space even significantly better.

5.4.3 Design Variants

Because of the large bending radius of high momentum tracks ($p \approx 50$ MeV/c) in the central region of the experiment, the bending angle of these tracks is significantly larger than 180° and does not provide optimal momentum resolution. This problem can be solved by adding a third cylinder of double pixel layers in the central region, see Fig. 10. Assuming that these extra layers can be added without adding a significant amount of support material in the active volume of the detector, the momentum resolution has been recalculated and is shown in Fig. 9 right. Compared to the two-cylinder design a clear improvement of the momentum resolution is seen in most of the regions of phase space. Due to the smaller radius of the second cylinder also the acceptance of low momentum tracks is improved.

5.5 Pixel Detector

The proposed tracking detector consists of two (or optionally three) concentric double layers of pixel sensors in the central region plus additional recurl stations of pixel sensors placed downstream and upstream. The optimal radial position depends on the strength of the magnetic field and the lower momentum accept-

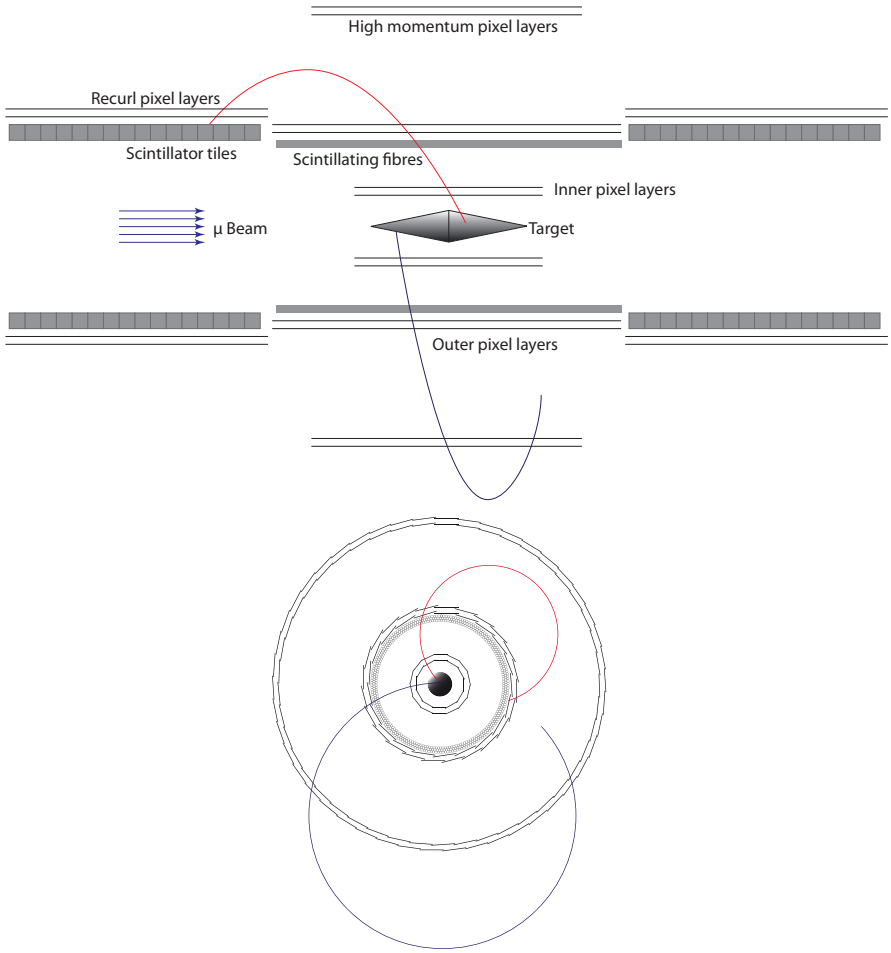

Figure 10: Schematic view of a design variant with a third double pixel layer added in the central region of the proposed experiment. Shown are the detector components in the side view (top) and in the transverse plane (bottom).

ance cut. The total detector length depends on the strength of the used magnet and lies between $1.5 - 1.8$ m, including the Recurl Stations.

For a pixel size of 80 μm everywhere, the tracker will consist of about 250 million pixels. The occupancy is highest for the inner detector layer, which should be placed as close as possible to the target to provide precise vertex position information. The signal rate at the inner most layer is at most 3 kHz per channel for a muon stop rate of $2 \cdot 10^9$ muons/s.

Timing information of pixel hits is exploited to ease track reconstruction and to reduce the combinatorial background. In order not to have more than 100 muon decay electrons to be reconstructed in the detector per readout frame, a hit resolution of 50 ns or better is required for the envisaged muon stopping rate of $2 \cdot 10^9$ muons/s.

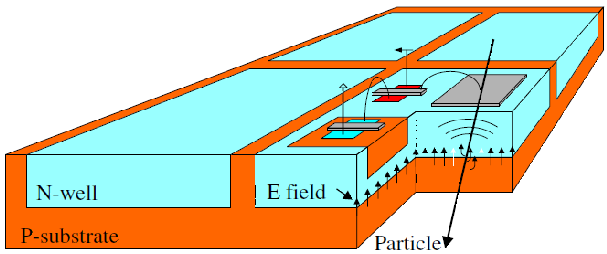

Figure 11: Sketch of the MAPS detector design from [70].

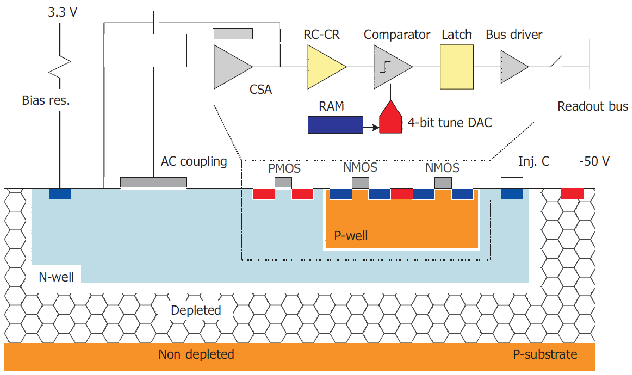

Figure 12: Block diagram of the HV MAPS detector from [70].

5.5.1 High Voltage MAPS Technology

We propose to use Monolithic Active Pixel Sensors (MAPS) as tracking detectors, as they integrate sensor and readout functionalities in the same device and thus greatly reduce the material budget. Classical concepts like hybrid designs usually have a higher material budget due to additional interconnects (bonds) and extra readout chips, which downgrade the track reconstruction performance, especially at low track momentum.

First MAPS designs were such that ionisation charges were collected mainly by diffusion, with a timing constant of several hundreds of nanoseconds. HV-MAPS designs with high bias voltages exceeding 50 V, however, overcome this problem and provide timing resolutions of better than 100 ns. We propose to use the High Voltage MAPS (HV-MAPS) design with pixel electronics completely implemented inside the deep N-well, which was first proposed by [70] and has since been successfully tested [71, 72]. Figure 11 shows a sketch of the proposed Monolithic Pixel Detector. The readout circuitry, see Fig. 12, allows an efficient zero suppression of pixel information and the implementation of timestamps to facilitate the assignments of hits between different pixel layers. For readout designs providing 50 ns timing resolutions power consumptions of about 150 mW/cm^2 are expected [73].

Because of the small size of the active depletion zone, the detectors can also be thinned down to 50 µm or less, depending on the complexity and vertical size of the readout circuitry. By "thinning", the material budget can be significantly

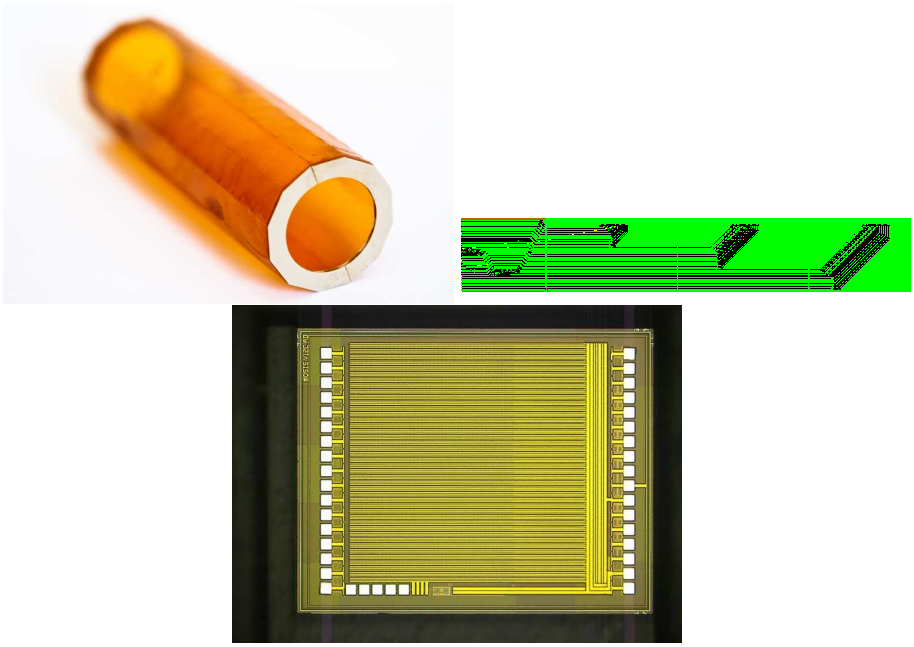

Figure 13: Photographs of the barrel support structure consisting of 25 µm Kapton, a silicon test structure in a 180 nm AMS process and a flexible print prototype design.

reduced and becomes comparable to tracking systems using gaseous detectors.

A further advantage is that MAPS can be implemented in the "cheap" CMOS process (e.g. AMS 180 nm), which also benefits from a high availability. A first test chip using the AMS 180 nm process was recently produced and successfully tested in Heidelberg.

5.5.2 Cooling and Mechanics

In order to reduce the effect of multiple scattering the support structures of the pixel detector must be placed mainly outside of the active volume. The detector is placed in a helium atmosphere which also serves as a coolant.

The main requirements for the mechanical support are to provide a rigid structure for the thin and flexible sensors and to add no significant mass to the material budget.

The baseline design uses a 25 µm thin kapton foil for mechanical support on which the sensors are glued. This foil serves also as a flexible print providing electrical connections for power and readout.

A photograph of the support structure and of the flexible print is shown in Fig. 13.

5.5.3 Alternative Technologies

In the following, several alternative technologies for the pixel sensor are discussed, with emphasis on the timing and the material budget.

Standard (non-high voltage) MAPS sensors [74] have been produced with thicknesses as small as 50 μm in a standard CMOS process and benefit from a high availability and low cost. However, the charge collection process is mainly based on diffusion, which is significantly slower than the charge collection by drifting in a high voltage sensor. Therefore, this technology has been disregarded for a high rate experiment such as *Mu3e*, since it does not fulfill the timing requirements.

The DEPFET [75,76] technology, which is currently being further developed for the *Belle II* experiment at KEK, features a small sensor thickness of 50 μm and small pixel sizes. This technology also provides an excellent signal-to-noise ratio. However, the readout is based on the "rolling shutter" method, which downgrades the time resolution and makes the use in a high rate experiment impossible.

The requirements on the timing resolution and fast readout are best fulfilled by hybrid pixel detectors, as developed for the LHC experiment *ATLAS*, *CMS* and *LHCb* and their planned upgrades, providing a time resolution of 25 ns or better. These sensors are however all developed in radiation hard technology, which is not a requirement for the *Mu3e* experiment. With a pixel size of 55×55 μm^2 the VELOPIX sensor developed for the *LHCb* vertex detector upgrade might be the best alternative. The power consumption has been estimated to be $1 - 1.5$ W/cm^2 at 40 MHz operation, this is considered to be too high to allow for air-cooling. Therefore, these sensors would have to be operated at a lower clock frequency. The VELOPIX sensor is 300 μm thick and needs a separate readout chip which is connected by metal bump bonds, leading to an unacceptable amount of material and multiple scattering.

In order to achieve the highest sensitivity the material budget of the hybrid pixel detectors would have to be lowered. It has been shown that similar pixel sensors can be efficiently operated after "thinning" to $150 - 200$ μm. Also the readout chip would have to be thinned down to a similar thickness. Several groups have recently started to investigate the capacitive coupling between the sensor and readout chips, thus avoiding (most) metal bump bonds. A successful combination of the above measures could reduce the material budget to between 300 - 400 μm of silicon and would provide an alternative for the phase I of the *Mu3e* experiment with an aimed sensitivity of 10^{-15}.

5.6 Time-of-Flight Hodoscope

The silicon tracker is complemented by scintillating fiber hodoscopes and scintillating tiles coupled to silicon photomultipliers (SiPM). The main task of the time-of-flight (ToF) system is to measure very precisely the time of arrival of particles in order to allow the matching with hits detected in the silicon vertex detector and to reject pile-up events. The ToF system will operate at very high particle rates (order 1 MHz). As illustrated in Fig. 8 the ToF system is composed of a central scintillating fiber (SciFi) hodoscope, cylindrical in shape, with a radius of about 6 cm and about 35 cm long. The recurling tracks will be measured by scintillating tiles, arranged also in a cylindrical shape, upstream and downstream of the central SciFi hodoscope.

The thickness of the hodoscope is of order 1 mm. This is also the thickness that will be seen by the outgoing electrons produced in muon decays, and has to be kept as low as possible, compatible with the proposed performance of this

sub-detector. The use of 200 - 250 micron fibers is envisaged. Several SciFi planes will be staggered such as to minimize empty spaces between fibers.

The scintillating light produced in the fibers will be detected with arrays of silicon photomultipliers (SiPM) at both fiber ends. The choice of SiPMs as a photodetection device is based on the fact that they are very compact detectors that can be operated in high magnetic fields with high gain ($\sim 10^6$) and at high counting rates (> 1 MHz). Typical dimensions of such SiPM arrays available from Hamamatsu [77, 78] are ~ 8 mm wide and 1 mm high, with 50×50 μm^2 or 100×100 μm^2 pixels. The pixels are arranged in columns, corresponding to an effective readout pitch of 250 microns. The photodetectors would be directly coupled to the SciFi arrays to maximize the light collection efficiency. Alternatively, the SciFis could be coupled to optical fibers to transport the scintillating light outside of the solenoid, where they would be coupled to the same SiPMs. To readout the fiber hodoscope at each end a total of 128 such photodetectors will be required corresponding to about 4000 readout channels.

For this central ToF detector we aim at a time resolution of few 100 ps. Time resolutions of about 200 ps have already been achieved with SciFi hodoscopes with single-sided readout using multianode PMTs [79]. In the design and construction of this detector it will be very important to maximize the photon detection efficiency of the photodetector in order to maximize the time resolution.

Recurling tracks, upstream and downstream of the central detector, will be measured with scintillating tiles, also coupled to SiPMs. The tiles of size $10 \times 10 \times 5$ mm^3 will be coupled to SiPMs of 1×1 mm^2 or 3×3 mm^2 with conical focusing light guides. About 3000 scintillating tiles, placed inside the cylindrical double-layers of the pixel detector, are required for each end of the solenoid. The tile ToF detector should achieve a time resolution of about 50 ps.

The granularity of the system (fibers and tiles) will be such that the single channel event rate is kept below 1 MHz. A total of about 10,000 readout channels is foreseen (4000 for the SciFi hodoscope, 6000 for the tile hodoscope). A vigorous R&D programme is being planned for the next two years to achieve the desired performances of the ToF system. The R&D activity will cover all the aspects of the ToF detector development: scintillators, SiPMs, and front end electronics. It is also planned to develop SiPMs that will match precisely the requirements of the ToF system.

5.6.1 Readout of Scintillating Fibres and Tiles

For the readout of the fibers and tiles it is planned to use the well-established waveform digitizing technology used already in the *MEG* experiment. This technology is based on the switched capacitor array chip DRS4 developed at PSI, which is capable of sampling the SiPM signal with up to 5 Giga samples per second with a resolution close to 12 bits. The advantage of this technology compared to traditional constant fraction discriminators and TDCs is that pile-up can be effectively recognized and corrected for. In addition, pulse height information becomes available which can be used to discriminate signals. To cope with the high rates expected during the second phase of the experiment a new version of the chip, the DRS5, see Fig. 14, capable of sustaining continuous rates of 2 MHz will be developed by the same PSI group. With the DRS5 the waveform segments will be read out and digitized continuously. A prototype of

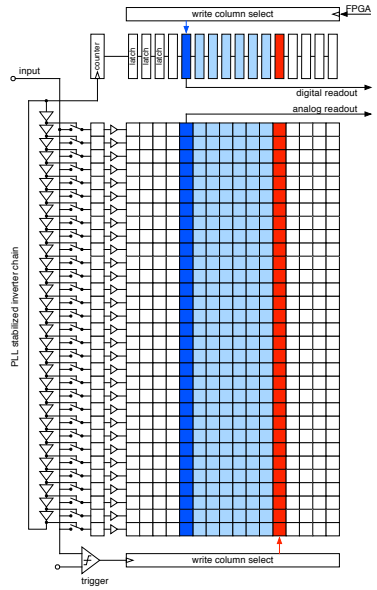

Figure 14: Simplified schematics of the DRS5 chip. A primary sampling array on the left side records a short segment of the input waveform, which is then transferred to the secondary sampling matrix on the right side. The switching of the sampling columns occur instantly, so no dead time occurs.

the DRS5 chip is planned for mid 2012, and the final chip will be available in time for the second phase of the experiment.

5.7 Readout and Online Reconstruction

Both the pixel detector and the fiber tracker contribute significantly to the data bandwidth of the experiment. The number of channels is basically given by the aimed resolution and the size of the detectors. Assuming four layers of silicon sensors with an 80 μm $\times$ 80 μm pixel size would give about 250 million channels for the tracking detector. Depending on the exact size and specification of the TOF system about 10000 channels should be considered for readout. A typical muon decay event has only one charged track (electron) in the final state. Assuming a muon stop rate of $2 \cdot 10^9$ per second the total data rate is estimated to be 50 GByte/s. This data rate puts some constraints on the front-end system and on the data links to the backend. However, using modern readout technologies the experiment can be operated without any hardware triggers. For data storage a reduction of a factor 1000 in bandwidth should be achieved using an online filter farm which implements very fast track reconstruction algorithms and requires a high degree of parallelism.

The main task of the filter farm is the fast reconstruction of tracks, track linking and event reconstruction. This can be implemented by using parallel processing nodes equipped with powerful Graphics Processing Units. The track reconstruction algorithm will use Kálmán filter or broken line fits in order to take the dominating multiple scattering into account.

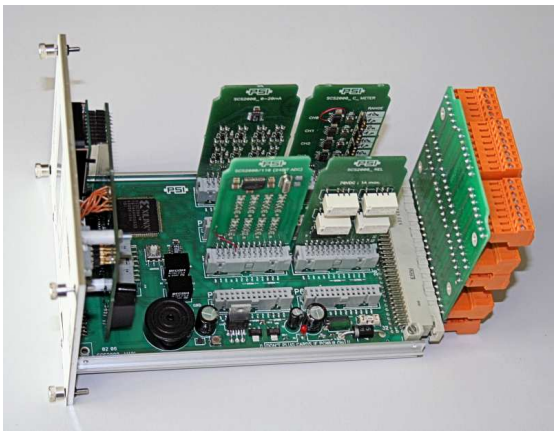

Figure 15: SCS-2001 unit as part of the MSCB slow control system. This unit has 64 input/output channels, which can be configured via plug-in boards as digital or analog channels. Many plug-in boards exist already such as PT100 temperature sensor readout cards, analog high resolution inputs (24 bit resolution), valve control outputs and many more.

5.8 Data collection

The filter farm will output selected events at a data rate in the order of 50 MBytes/s in total. This data rate is low enough to be collected by a single PC connected to the filter farm by common GBit Ethernet and written to local disks. Then the data will be transferred to the central PSI computing center, where it is stored and analyzed. The resulting annual data volume of about 500 TB can be accommodated already by the existing infrastructure of disk and tape arrays at PSI. If running for several years, one can always reduce the data by analyzing it offline and keeping only events of interest. For the data acquisition the well-established MIDAS [80] system will be used. This system is currently used in several major experiments such as the *T2K ND280* detector in Japan [44], ALPHA at CERN and the *MEG* experiment at PSI [17]. It can easily handle the required data rate, and contains all necessary tools such as event building, a slow control system including a history database and an alarm system. A web interface allows controlling and monitoring the experiment through the internet.

5.9 Slow Control System

The slow control system deals with all "slow" data such as high voltages for the SiPMs and silicon sensors, ambient temperatures and pressures. For the configuration and control of the silicon pixel sensors JTAG [81] will be used.

It is planned to use the MIDAS Slow Control Bus (MSCB) system [82] to link all distributed control and monitoring devices into a single system. The MSCB system is also well established at several laboratories. It uses a serial differential bus for communication, and simple micro controllers in all control devices. The micro controllers perform local control loops such as high voltage stabilisation, and send measured values to the central DAQ system for monitoring. Many devices already exist for this system, such as the SCS-2001 unit

shown in Fig. 15. Since the system was developed at PSI, it can be quickly adapted to new hardware. The high voltage control for the SiPMs can for example be directly integrated into the carrier boards holding the SiPMs, thus eliminating the need for high voltage cables. The optimized protocol of the MSCB system allows the monitoring of many thousand channels with repetition rates in the 100 ms range, which will be more than enough for this experiment. All slow control data will be stored in the history system of the MIDAS system, so that long term stabilities of the experiment can be effectively verified. The slow control data is also fed into the main event data stream, so that any offline analysis of the event data has this data available.

	Phase I	Phase II
Year	2014-2017	> 2017
Muon Rate/s	$2 \cdot 10^8$	$2 \cdot 10^9$
Total Running Time	350 days	350 days
Stopped-Muon Decays	$3 \cdot 10^{15}$	$3 \cdot 10^{16}$
Exp. Background	0	0
Detector Acceptance	0.7	0.7
Detector Efficiency	0.7	0.7
Sensitivity (90% CL)	10^{-15}	10^{-16}

Table 4: Breakdown of the sensitivity calculation for the two phases of the experiment

6 Timetable, Task Lists and Institutional Responsibilities

6.1 Timetable

The schedule for reaching the final sensitivity of $\mathrm{B}(\mu^+ \to e^+e^-e^+) < 10^{-16}$ is mainly driven by the availability of the high intensity muon beam, which has to provide $> 10^9$ muon stops per second and requires either larger modifications of existing beamlines or the installation of a new beamline e.g. at the SINQ target. Therefore, we propose to perform the experiment in two phases, see table 4, after an initial phase of beam tests (2012-2013).

In the first phase (2014-2017) we will use an existing beamline at the "E" target of the PSI proton cyclotron, providing at minimum 10^8 muon stops per second. The detector could be installed in the PiE5 beamline area after the *MEG* experiment has finalised data taking or share this area in case that the *MEG* is continued beyond 2012. At this intensity the accidental background rate will be small and the requirements on the timing resolution of the experiment are expected to be moderate. This experiment will be able to test sensitivities of $\mathrm{B}(\mu^+ \to e^+e^-e^+) = 10^{-15}$.

In the second phase ≥ 2017 the experiment could be continued at an upgraded or even new beamline with one order of magnitude increased beam intensity ($\gtrsim 10^9$ muon stops per second). To fully exploit the high beam intensity, the requirements on the detector for background reduction, concerning energy and timing resolution, are more severe. The use of a scintillating fibre hodoscope for precise timing measurements will be inevitable. Experience and knowledge gathered at the first running period of this experiment will certainly help to improve the experimental design.

6.2 Tasks and Institutional Responsibilities

6.2.1 Beamline

In the first phase of the experiment (>2013) an existing beamline can be used. In case that the PiE5 area has to be shared with the *MEG* experiment larger modifications are required. For the second phase an upgraded or new beam-

line providing more than $2 \cdot 10^9$ muons per second has to be newly installed. The design and construction of the beam line will be collaborative effort by all involved partners and managed under the leadership of PSI.

6.2.2 Target

The use of passive or active beam targets to stop the muons is presently subject of studies and will be defined at a later phase of the project. Heidelberg and PSI are interested to take responsibility for the target.

6.2.3 Magnet

The magnet has to provide a solenoidal field of B = 1-1.5 Tesla and should be preferably superconducting in order to reduce maintenance costs. The proponents are currently searching for interested parties and groups willing to take responsibility for the magnet design and construction.

6.2.4 Silicon Tracker

The silicon tracker based on the HV-MAPS technology is developed by the ZITI Mannheim and the Uni Heidelberg. Heidelberg and the ETH Zurich are interested to take the responsibiity for the construction of the multi-layer silicon detector and the recurling stations. The responsibility includes also the design of the frontend readout system.

6.2.5 Time-of-Flight Hodoscopes

The time-of-flight hodocsopes, based on scintillating fibers and tiles with SiPMs for photon detection are developed and constructed by Uni Geneva and Uni Zurich. The readout will be developed in close collaboration with the PSI.

6.2.6 Filter Farm / Online Reconstruction

The software filter farm providing a fast online reconstruction for event selection is in the responsibility of the Uni Heidelberg. All participating groups are expected to contribute to the hardware and software algorithms.

6.2.7 Data Acquisition and Slow Control

The data acquisition system including the data management and storage, and the slow control is in the responsibility of the PSI group.

6.2.8 Data Analysis and Simulation

It is expected that all participating groups are contributing to the data analysis and simulations.

6.3 Costs

The estimated costs for the proposed experiment are listed in Table 5 for the two phases of the experiment.

Task	Phase I Costs [kCHF]	Phase II Costs [kCHF]
Target + Infrastructure	50	50
Magnet	1000	0
Silicon Tracker	500	200
Fibre Hodoscope	400	200
Filter Farm	300	300
DAQ + Slow Control	500	500
Beamline	u.a.	u.a.

Table 5: Estimated costs for the two phases of the experiment. (u.a.= under assessment).

The total costs for the detector in the first phase of the experiment not counting running costs and personpower are estimated to be of the order of 2.75 million Francs. In the second phase costs for the detector upgrade are of the order of 1.25 million Francs. The costs for the beamline are currently under assessment.

References

[1] Y. Fukuda et al., [Super-Kamiokande Collaboration], *"Evidence for oscillation of atmospheric neutrinos"*, Phys. Rev. Lett., **81** 1562–1567, 1998.

[2] Q. R. Ahmad et al., [SNO Collaboration], *"Measurement of the charged current interactions produced by B-8 solar neutrinos at the Sudbury Neutrino Observatory"*, Phys. Rev. Lett., **87** 071301, 2001.

[3] K. Eguchi et al., [KamLAND Collaboration], *"First results from KamLAND: Evidence for reactor anti- neutrino disappearance"*, Phys. Rev. Lett., **90** 021802, 2003.

[4] J. C. Pati and A. Salam, *"Lepton Number as the Fourth Color"*, Phys. Rev., **D10** 275–289, 1974.

[5] H. Georgi and S. L. Glashow, *"Unity of All Elementary Particle Forces"*, Phys. Rev. Lett., **32** 438–441, 1974.

[6] P. Langacker, *"Grand Unified Theories and Proton Decay"*, Phys.Rep., **72** 185, 1981.

[7] H. E. Haber and G. L. Kane, *"The Search for Supersymmetry: Probing Physics Beyond the Standard Model"*, Phys. Rept., **117** 75, 1985.

[8] R. N. Mohapatra and J. C. Pati, *"Left-Right Gauge Symmetry and an Isoconjugate Model of CP Violation"*, Phys. Rev., **D11** 566–571, 1975.

[9] R. N. Mohapatra and J. C. Pati, *"A Natural Left-Right Symmetry"*, Phys. Rev., **D11** 2558, 1975.

[10] G. Senjanovic and R. N. Mohapatra, *"Exact Left-Right Symmetry and Spontaneous Violation of Parity"*, Phys. Rev., **D12** 1502, 1975.

[11] M. Kakizaki, Y. Ogura and F. Shima, *"Lepton flavor violation in the triplet Higgs model"*, Phys.Lett., **B566** 210–216, 2003.

[12] C. T. Hill and E. H. Simmons, *"Strong dynamics and electroweak symmetry breaking"*, Phys. Rept., **381** 235–402, 2003.

[13] L. Randall and R. Sundrum, *"A large mass hierarchy from a small extra dimension"*, Phys. Rev. Lett., **83** 3370, 1999.

[14] N. Arkani-Hamed and M. Schmaltz, *"Hierarchies without symmetries from extra dimensions"*, Phys. Rev., **D61** 33005, 2000.

[15] M. L. Brooks et al., [MEGA Collaboration], *"New limit for the family-number non-conserving decay $\mu^+ rightarrow e^+\gamma$"*, Phys. Rev. Lett., **83** 1521–1524, 1999.

[16] D. Nicolo, [MEG Collaboration], *"The $\mu \to e\gamma$ experiment at PSI"*, Nucl.Instrum.Meth., **A503** 287–289, 2003.

[17] J. Adam et al., [MEG collaboration], *"A limit for the $\mu \to e\gamma$ decay from the MEG experiment"*, Nucl.Phys., **B834** 1–12, 2010.

[18] J. Adam et al., [MEG], *"New limit on the lepton-flavour violating decay mu -> e gamma"*, Phys. Rev. Lett., **107** 171801, 2011.

[19] U. Bellgardt et al., [SINDRUM Collaboration], *"Search for the Decay $\mu^+ \to e^+e^+e^-$"*, Nucl.Phys., **B299** 1, 1988.

[20] Wilhelm H. Bertl et al., [SINDRUM II], *"A Search for $\mu - e$ conversion in muonic gold"*, Eur. Phys. J., **C47** 337–346, 2006.

[21] J. P. Lees et al., [BaBar Collaboration], *"Limits on tau Lepton-Flavor Violating Decays in three charged leptons"*, Phys. Rev., **D81** 111101, 2010.

[22] B. Aubert et al., [BaBar Collaboration], *"Searches for Lepton Flavor Violation in the Decays $\tau \to e\gamma$ and $\tau \to \mu\gamma$"*, Phys. Rev. Lett., **104** 021802, 2010.

[23] B. Aubert et al., [BaBar Collaboration], *"Improved limits on lepton flavor violating tau decays to $\ell\phi$, $\ell\rho$, ℓK^* and $\ell\bar{K}^*$"*, Phys. Rev. Lett., **103** 021801, 2009.

[24] B. Aubert et al., [BaBar Collaboration], *"Search for Lepton Flavour Violating Decays $\tau \to \ell K^0_S$ with the BaBar Experiment"*, Phys. Rev., **D79** 012004, 2009.

[25] B. Aubert et al., [BaBar Collaboration], *"Search for Lepton Flavor Violating Decays $\tau^\pm \to \ell^\pm\omega$ $(\ell = e, \mu)$"*, Phys. Rev. Lett., **100** 071802, 2008.

[26] B. Aubert et al., [BaBar Collaboration], *"Search for Lepton Flavor Violating Decays $\tau^\pm \to \ell^\pm\pi^0, \ell^\pm\eta, \ell^\pm\eta'$"*, Phys. Rev. Lett., **98** 061803, 2007.

[27] K. Hayasaka et al., [Belle Collaboration], *"Search for Lepton Flavor Violating τ Decays into Three Leptons with 719 Million Produced $\tau^+\tau^-$ Pairs"*, Phys. Lett., **B687** 139–143, 2010.

[28] Y. Miyazaki et al., [Belle Collaboration], *"Search for Lepton Flavor Violating τ^- Decays into $\ell^- K^0_s$ and $\ell^- K^0_s K^0_s$"*, Phys. Lett., **B692** 4–9, 2010.

[29] Y. Miyazaki et al., [Belle Collaboration], *"Search for Lepton Flavor and Lepton Number Violating tau Decays into a Lepton and Two Charged Mesons"*, Phys. Lett., **B682** 355–362, 2010.

[30] Y. Miyazaki et al., [Belle Collaboration], *"Search for Lepton-Flavor-Violating tau Decays into Lepton and $f_0(980)$ Meson"*, Phys. Lett., **B672** 317–322, 2009.

[31] Y. Miyazaki et al., [Belle Collaboration], *"Search for Lepton Flavor Violating tau Decays into Three Leptons"*, Phys. Lett., **B660** 154–160, 2008.

[32] Y. Nishio et al., [Belle Collaboration], *"Search for lepton-flavor-violating $\tau \to \ell V^0$ decays at Belle"*, Phys. Lett., **B664** 35–40, 2008.

[33] Y. Miyazaki et al., [Belle Collaboration], *"Search for lepton flavor violating τ^- decays into $\ell^-\eta$, $\ell^-\eta'$ and $\ell^-\pi^0$"*, Phys. Lett., **B648** 341–350, 2007.

[34] Y. Miyazaki et al., [Belle Collaboration], *"Search for lepton flavor violating tau-decays with a K^0_S meson"*, Phys. Lett., **B639** 159–164, 2006.

[35] Y. Kuno and Y. Okada, *"Muon decay and physics beyond the standard model"*, Rev. Mod. Phys., **73** 151–202, 2001.

[36] L. Calibbi, A. Faccia, A. Masiero and S.K. Vempati, *"Lepton flavour violation from SUSY-GUTs: Where do we stand for MEG, PRISM/PRIME and a super flavour factory"*, Phys.Rev., **D74** 116002, 2006.

[37] S. Antusch, E. Arganda, M.J. Herrero and A.M. Teixeira, *"Impact of theta(13) on lepton flavour violating processes within SUSY seesaw"*, JHEP, **0611** 090, 2006.

[38] G. Aad et al., [ATLAS], *"Searches for supersymmetry with the ATLAS detector using final states with two leptons and missing transverse momentum in sqrts = 7 TeV proton-proton collisions"*, 2011, arXiv:1110.6189 [hep-ex].

[39] G. Aad et al., [ATLAS], *"Search for supersymmetry in final states with jets, missing transverse momentum and one isolated lepton in sqrts = 7 TeV pp collisions using 1 fb-1 of ATLAS data"*, 2011, arXiv:1109.6606 [hep-ex].

[40] G. Aad et al., [ATLAS Collaboration], *"Search for squarks and gluinos using final states with jets and missing transverse momentum with the ATLAS detector in sqrt(s) = 7 TeV proton-proton collisions"*, 2011, arXiv:1109.6572 [hep-ex].

[41] S. Chatrchyan et al., [CMS], *"Search for Supersymmetry at the LHC in Events with Jets and Missing Transverse Energy"*, Phys. Rev. Lett., **107** 221804, 2011.

[42] B.C. Allanach, M. Battaglia, G.A. Blair, Marcela S. Carena, A. De Roeck et al., *"The Snowmass points and slopes: Benchmarks for SUSY searches"*, Eur.Phys.J., **C25** 113–123, 2002.

[43] M. Mezzetto and T. Schwetz, *"Theta$_{13}$: Phenomenology, present status and prospect"*, J.Phys., **G37** 103001, 2010.

[44] K. Abe et al., [T2K Collaboration], *"Indication of Electron Neutrino Appearance from an Accelerator-produced Off-axis Muon Neutrino Beam"*, Phys. Rev. Lett., **107** 041801, 2011.

[45] P. Adamson et al., [MINOS Collaboration], *"Improved search for muon-neutrino to electron-neutrino oscillations in MINOS"*, 2011.

[46] H. De Kerrect, talk given at the 6th International Workshop on Low Energy Neutrino Physics, LowNu2011, 9-12, November, 2011, Seoul National University, available from `http://workshop.kias.re.kr/lownu11/`.

[47] P.A.N. Machado, H. Minakata, H. Nunokawa and R.Zukanovich Funchal, *"Combining Accelerator and Reactor Measurements of θ_{13}: The First Result"*, 2011, arXiv:1111.3330 [hep-ph].

[48] Y. Okada, K. Okumura and Y. Shimizu, *"$\mu \to e\gamma$ and $\mu \to 3e$ processes with polarized muons and supersymmetric grand unified theories"*, Phys.Rev., **D61** 094001, 2000.

[49] M. Blanke, A. J. Buras, B. Duling, A. Poschenrieder and C. Tarantino, *"Charged Lepton Flavour Violation and (g-2)(mu) in the Littlest Higgs Model with T-Parity: A Clear Distinction from Supersymmetry"*, JHEP, **0705** 013, 2007.

[50] M. Blanke, A. J. Buras, B. Duling, S. Recksiegel and C Tarantino, *"FCNC Processes in the Littlest Higgs Model with T-Parity: a 2009 Look"*, Acta Phys. Polon., **B41** 657–683, 2010.

[51] W.F. Chang and J. N. Ng, *"Lepton flavor violation in extra dimension models"*, Phys.Rev., **D71** 053003, 2005.

[52] S. Casagrande, F. Goertz, U. Haisch, M. Neubert and T. Pfoh, *"Flavor Physics in the Randall-Sundrum Model: I. Theoretical Setup and Electroweak Precision Tests"*, JHEP, **10** 094, 2008.

[53] M. S. Carena, A. Delgado, E. Ponton, T. M. P. Tait and C. E. M. Wagner, *"Precision electroweak data and unification of couplings in warped extra dimensions"*, Phys. Rev., **D68** 035010, 2003.

[54] A. Delgado and A. Falkowski, *"Electroweak observables in a general 5D background"*, JHEP, **05** 097, 2007.

[55] W. Bertl, SINDRUM I, Presentation at PSI, 2008.

[56] J. Kaulard et al., [SINDRUM II Collaboration], *"Improved limit on the branching ratio of $\mu^- \to e^+$ conversion on titanium"*, Phys.Lett., **B422** 334–338, 1998.

[57] C. Dohmen et al., [SINDRUM II Collaboration], *"Test of lepton flavor conservation in $\mu \to e$ conversion on titanium"*, Phys. Lett., **B317** 631–636, 1993.

[58] R.M. Carey et al., [Mu2e Collaboration], *"Proposal to search for mu- N -> e- N with a single event sensitivity below 10 -16"*, 2008, Spokespersons: J.P. Miller, R.H. Bernstein.

[59] R. Tschirhart, *"The Mu2e experiment at Fermilab"*, Nucl.Phys.Proc.Suppl., **210-211** 245–248, 2011.

[60] Y.G. Cui et al., [COMET Collaboration], *"Conceptual design report for experimental search for lepton flavor violating mu- - e- conversion at sensitivity of 10^{-16} with a slow-extracted bunched proton beam (COMET)"*, 2009.

[61] Yoshitaka Kuno, [COMET Collaboration], *"Search for muon to electron conversion at J-PARC: COMET"*, PoS, **ICHEP2010** 526, 2010.

[62] Yoshitaka Kuno, *"Lepton flavor violation: Muon to electron conversion, COMET and PRISM/PRIME at J-PARC"*, PoS, **NUFACT08** 111, 2008.

[63] J. Pasternak, L. Jenner, Y. Uchida, R. Barlow, K. Hock et al., *"Accelerator and Particle Physics Research for the Next Generation Muon to Electron Conversion Experiment - the PRISM Task Force"*, **WEPE056**, 2010.

[64] K Nakamura et al., [Particle Data Group], *"Review of particle physics"*, J. Phys., **G37** 075021, 2010.

[65] R. M. Djilkibaev and R. V. Konoplich, *"Rare Muon Decay $\mu^+ \to e^+e^-e^+\nu_e\bar{\nu_\mu}$"*, Phys.Rev., **D79** 073004, 2009.

[66] P.-R. Kettle, PSI-internal, LTP Filzbach Meeting, June 2010.

[67] S. Agostinelli et al., *"G4–a simulation toolkit"*, Nucl. Instr. Meth., **A 506**(3) 250 – 303, 2003.

[68] John Allison, K. Amako, J. Apostolakis, H. Araujo, P.A. Dubois et al., *"Geant4 developments and applications"*, IEEE Trans.Nucl.Sci., **53** 270, 2006.

[69] A. Schöning, Multiple scattering dominated tracking, Technical report, Internal Note, 2010.

[70] I. Peric, *"A novel monolithic pixelated particle detector implemented in high-voltage CMOS technology"*, Nucl.Instrum.Meth., **A582** 876–885, 2007.

[71] I. Peric and C. Takacs, *"Large monolithic particle pixel-detector in high-voltage CMOS technology"*, Nucl. Instrum. Meth., **A624**(2) 504 – 508, 2010, New Developments in Radiation Detectors - "Proceedings of the 11th European Symposium on Semiconductor Detectors, 11th European Symposium on Semiconductor Detectors".

[72] I. Peric, C. Kreidl and P. Fischer, *"Particle pixel detectors in high-voltage CMOS technology–New achievements"*, Nucl. Instrum. Meth. A, **In Press, Corrected Proof** –, 2010.

[73] I. Peric, Private communication, 2010.

[74] R. Turchetta, J.D. Berst, B. Casadei, G. Claus, C. Colledani et al., *"A monolithic active pixel sensor for charged particle tracking and imaging using standard VLSI CMOS technology"*, Nucl.Instrum.Meth., **A458** 677–689, 2001.

[75] J. Ulrici et al., *"Spectroscopic and imaging performance of DEPFET pixel sensors"*, Nucl. Instrum. Meth., **A465** 247–252, 2000.

[76] P. Fischer et al., *"Progress towards a large area, thin DEPFET detector module"*, Nucl. Instrum. Meth., **A582** 843–848, 2007.

[77] B. Beischer et al., *"A high-resolution scintillating fiber tracker with silicon photomultiplier array readout"*, Nucl.Instrum.Meth., **A622** 542–554, 2010.

[78] B. Beischer et al., *"The development of a high-resolution scintillating fiber tracker with silicon photomultiplier readout"*, Nucl.Instrum.Meth., **A628** 403–406, 2011.

[79] P. Abbon et al., [COMPASS Collaboration], *"The COMPASS experiment at CERN"*, Nucl.Instrum.Meth., **A577** 455–518, 2007.

[80] K. Olchanski S. Ritt, P. Amaudruz, Maximum Integration Data Acquisition System, 2001, `http://midas.psi.ch`.

[81] Institute of Electrical and Electronics Engineers, *IEEE 1149.1: Standard Test Access Port and Boundary Scan Architecture*, 2001.

[82] R. Schmidt S. Ritt, MSCB (MIDAS Slow Control Bus), 2001, `http://midas.psi.ch/mscb`.